

# Semiclassical Distorted Wave Model Analysis of Backward Proton Emission from $(p, p'x)$ Reactions at Intermediate Energies

M.K. Gaidarov<sup>a,b</sup>, Y. Watanabe<sup>a</sup>, K. Ogata<sup>c</sup>,  
 M. Kohno<sup>d</sup>, M. Kawai<sup>c</sup>, A.N. Antonov<sup>b</sup>

<sup>a</sup>*Department of Advanced Energy Engineering Science,  
 Kyushu University, Kasuga, Fukuoka 816-8580, Japan*

<sup>b</sup>*Institute of Nuclear Research and Nuclear Energy,  
 Bulgarian Academy of Sciences, Sofia 1784, Bulgaria*

<sup>c</sup>*Department of Physics, Kyushu University,  
 Fukuoka 812-8581, Japan*

<sup>d</sup>*Physics Division, Kyushu Dental College,  
 Kitakyushu 803-8580, Japan*

A semiclassical distorted wave (SCDW) model with Wigner transform of one-body density matrix is presented for multistep direct  $(p, p'x)$  reactions to the continuum. The model uses Wigner distribution functions obtained in methods which include nucleon-nucleon correlations to a different extent, as well as Woods-Saxon (WS) single-particle wave function. The higher momentum components of target nucleons that play a crucial role in reproducing the high-energy part of the backward proton spectra are properly taken into account. This SCDW model is applied to analyses of multistep direct processes in  $^{12}\text{C}(p, p'x)$ ,  $^{40}\text{Ca}(p, p'x)$  and  $^{90}\text{Zr}(p, p'x)$  in the incident energy range of 150–392 MeV. The double differential cross sections are calculated up to three-step processes. The calculated angular distributions are in good agreement with the experimental data, in particular at backward angles where the previous SCDW calculations with the WS single-particle wave function showed large underestimation. It is found that the result with the Wigner distribution function based on the coherent density fluctuation model provides overall better agreement with the experimental data over the whole emission energies.

## 1 Introduction

Preequilibrium processes in nuclear reactions at intermediate energies are known to be dominated by multistep direct (MSD) processes. Among the models proposed in the years, the semiclassical distorted wave model [1, 2, 3] has proved its efficiency to describe MSD, especially for reactions at intermediate energies. It is based on the DWBA expansion of  $T$ -matrix elements and the cross section formula has no free adjustable parameter allowing a simple intuitive interpretation. The SCDW model has been applied to analyses of inclusive cross sections and spin observables in  $(p, p'x)$  and  $(p, nx)$  reactions over incident energy region of 60 to 400 MeV and wide range of mass number [4, 5, 6, 7, 8]. Recently, several extensions and improvements of the SCDW model have been made. They include calculations up to three-step processes [4], incorporation of a single-particle (s.p.) wave function of target nuclei by using the Wigner transform of a one-body density matrix (OBDM) [5], introduction of phenomenological effective mass  $m^*$  of a nucleon in the target nucleus [6] and analyses of spin observables [7, 8] which contain important information on an effective interaction in nuclear medium. As a result, SCDW model calculations

can well reproduce the experimental data of double differential inclusive cross sections (DDX's) for  $(p, p'x)$  and  $(p, nx)$  reactions. The model, however, underestimated the cross sections at very backward angles. This suggests that improvement of the SCDW model might be achieved by the inclusion of the high momentum components of the target nucleons.

The problem of backward proton production in proton-nucleus collisions has been a subject of much interest for several years. The main difficulty arises from the fact that the reaction involves a very large momentum transfer with only a small energy transfer. One of the models which have been applied to solve the problem is based on the correlated two-nucleon-cluster picture [9]. A good description of the energy spectra even at the very high energy backward protons is achieved with this model. The main reason is that a phenomenological momentum distribution with high momentum components was employed [10]. These components were found to be quite sensitive to the problem of backward proton production and were considered to be an effect due to many-nucleon correlations. Within the model [9] single scattering and two-nucleon cluster mechanisms at backward angles have been considered. Although there are some similarities between these contributions and corresponding one- and two-step processes, the advantage of the SCDW model is that the contribution from three-step process can be also obtained. Moreover, in SCDW model the distortion effects for the projectile and observed protons are carefully considered within DWBA while the calculated single scattering mechanism in [9] has evaluated the distortion effect approximately by the Glauber theory.

In Ref. [5] the SCDW model was modified so that realistic s.p. wave functions in a finite range potential can be used in terms of the Wigner transform of OBDM. Single-particle models with harmonic oscillator and Woods-Saxon potentials were used to describe the nuclear states for  $^{90}\text{Zr}(p, p'x)$  reactions at 80 and 160 MeV instead of the local density Fermi gas (LFG) model used in previous analyses [4, 7]. It was concluded in [5] that the SCDW model with realistic s.p. wave functions gives larger one-step cross sections at backward angles, which result in better agreement with the experimental data over a wider angular range than the model with LFG. The calculations still somewhat underestimated the cross section at very large angles. Therefore, apart from the necessity of involving contributions of higher MSD processes the inclusion of higher momentum components of target nucleons becomes apparent. In the present paper we extend the SCDW model in terms of the Wigner transform of OBDM by considering the high-momentum components of nucleon momentum distributions deduced from several theoretical methods. This extended SCDW model is applied to  $^{12}\text{C}(p, p'x)$  reaction at 150 MeV [11, 12],  $^{40}\text{Ca}(p, p'x)$  reaction at 186 [13] and 392 MeV [14] and  $^{90}\text{Zr}(p, p'x)$  at 160 MeV [15] and comparison with the experimental data is made.

The aim of our work is to analyze the angular distributions of the backward scattered protons through testing of different models for the nuclear states which account for nucleon-nucleon (NN) correlations. Such a systematic study could lead to a further refinement of the SCDW model and to a better agreement of the DDX with the experimental data at backward angles due to a proper inclusion of high-momentum components of the nuclear Fermi motion.

The paper is organized as follows. A brief formulation of the SCDW model and the proposed WT within different theoretical models are given in Sections II and III, respectively. The results of the calculations are presented and discussed in Section IV. The summary of the present work is given in Section V.

## 2 Outline of the SCDW model

The formulation of the SCDW model used in the present analysis has been described in details elsewhere [5, 7, 8], therefore only the outline is mentioned here.

Let us consider the one-step process in  $(N, N'x)$  reactions in which a target nucleon is excited from an initial single particle state  $\alpha$  with the energy  $\varepsilon_\alpha$  to a final one  $\beta$  in the continuum with

the energy  $\varepsilon_\beta$ . A final expression of the inclusive  $(N, N'x)$  double differential cross section for the one-step process is given by

$$\frac{\partial^2 \sigma^{(1)}}{\partial E_f \partial \Omega_f} = \left( \frac{A}{A+1} \right)^2 \int d\mathbf{r} \frac{k_f/k_f(\mathbf{r})}{k_i/k_i(\mathbf{r})} |\chi_i^{(+)}(\mathbf{r})|^2 |\chi_f^{(-)}(\mathbf{r})|^2 \sum_\tau \left( \frac{\partial^2 \sigma}{\partial E_f \partial \Omega_f} \right)_\mathbf{r}^\tau \rho_\tau(\mathbf{r}), \quad (1)$$

where  $A$  is the target mass number,  $k_c$  and  $k_c(\mathbf{r})$  ( $c=i$  or  $f$ ) the wave number at infinity and the local wave number in the initial ( $i$ ) and final ( $f$ ) channels,  $\chi_i^+$  ( $\chi_f^-$ ) the distorted wave in the initial (final) channel, and  $\rho_\tau(\mathbf{r})$  ( $\tau=p$  or  $n$ ) the nucleon density for proton ( $p$ ) or neutron ( $n$ ) as the struck nucleon.

The local average nucleon-nucleon (NN) scattering cross section for collision between a leading particle,  $N$ , and a target nucleon,  $\tau$ , is given by

$$\begin{aligned} \left( \frac{\partial^2 \sigma}{\partial E_f \partial \Omega_f} \right)_\mathbf{r}^\tau &= \frac{2}{(2\pi)^3} \frac{1}{\rho_\tau(\mathbf{r})} \frac{k_f(\mathbf{r})}{k_i(\mathbf{r})} \int \int d\mathbf{k}_\alpha d\mathbf{k}_\beta f_h^\tau(\mathbf{k}_\alpha, \mathbf{r}) [2 - f_h^\tau(\mathbf{k}_\beta, \mathbf{r})] \\ &\times \left( \frac{\partial \sigma}{\partial \Omega} \right)_{N\tau} \delta(\mathbf{k}_f(\mathbf{r}) + \mathbf{k}_\beta - \mathbf{k}_i(\mathbf{r}) - \mathbf{k}_\alpha) \delta(\varepsilon_\beta - \varepsilon_\alpha - \omega), \end{aligned} \quad (2)$$

where  $\mathbf{k}_\alpha(\mathbf{k}_\beta)$  is the nucleon momentum for a single-particle state with the energy  $\varepsilon_\alpha(\varepsilon_\beta)$ ,  $\omega$  the energy transfer,  $(\partial \sigma / \partial \Omega)_{N\tau}$  the two-nucleon scattering cross section and  $f_h^\tau(\mathbf{k}, \mathbf{r})$  is the Wigner transform of the OBDM for the hole states of proton and neutron. In Eq. (2) the sum rule of the WT for the hole and particle states is used:

$$f_h(\mathbf{k}, \mathbf{r}) + f_p(\mathbf{k}, \mathbf{r}) = 2, \quad (3)$$

where  $f_p(\mathbf{k}, \mathbf{r})$  stands for the WT for the particle states. The factor  $f_h^\tau(\mathbf{k}_\alpha, \mathbf{r})[2 - f_h^\tau(\mathbf{k}_\beta, \mathbf{r})]$  in Eq. (2) represents the "probability" of the momentum state  $\hbar\mathbf{k}_\alpha$  being occupied and  $\hbar\mathbf{k}_\beta$  being unoccupied. The Pauli blocking effect is reflected in this factor. The difference between the single-particle energies in the second  $\delta$ -function in the right-hand side of Eq. (2) is given by

$$\varepsilon_\alpha - \varepsilon_\beta = \frac{\hbar^2}{2m^*(\mathbf{r})} [k_\beta^2(\mathbf{r}) - k_\alpha^2(\mathbf{r})], \quad (4)$$

using the effective mass of a nucleon,  $m^*(\mathbf{r})$  [16].

The extension to higher-step processes is straightforward and the same final expressions as in Ref. [4] with the local average NN scattering cross sections given by Eq. (2) for successive collision points are also deduced for two- and three-step processes.

### 3 Wigner transform of one-body density matrix using different theoretical models

We introduce formulae for the Wigner transform (WT) derived in some theoretical methods, namely calculated with WS s.p. wave function (denoted as WS), with natural orbitals (NO) obtained from the Jastrow correlation method (JCM) which accounts for short-range correlations (SRC) in the case of  $^{40}\text{Ca}$  (denoted as JCM), from the approach based on the local density approximation (LDA) including the effects of SRC (denoted as LDA+SRC) and from the coherent density fluctuation model (denoted as CDFM).

#### 3.1 WT with WS

For a single-particle potential, for instance Woods-Saxon potential, the WT for the hole states of proton or neutron is given by [5]

$$f_h^\tau(\mathbf{k}, \mathbf{r}) = \sum_{nlj} \frac{2j+1}{2l+1} \int_0^\infty d\mathbf{s} e^{-i\mathbf{k}\cdot\mathbf{s}} \sum_m \phi_{nlmj}^\tau(\mathbf{r} + \mathbf{s}/2) \phi_{nlmj}^{\tau*}(\mathbf{r} - \mathbf{s}/2), \quad (5)$$

where  $\phi_{nlmj}^\tau(\mathbf{r})$  is the s.p. wave function for the target nucleon and the sum runs over all the occupied orbits  $nlj$  of protons or neutrons.

### 3.2 WT with JCM

A model independent way to define a set of single-particle wave functions and occupation probabilities uniquely from the correlated OBDM  $\rho(\mathbf{r}, \mathbf{r}')$  is to use its natural orbital representation (NOR) [17]

$$\rho_{NOR}(\mathbf{r}, \mathbf{r}') = \sum_{\alpha} n_{\alpha} \psi_{\alpha}^*(\mathbf{r}) \psi_{\alpha}(\mathbf{r}'). \quad (6)$$

The normalized eigenfunctions  $\psi_{\alpha}(\mathbf{r})$  of  $\rho(\mathbf{r}, \mathbf{r}')$ , the so-called natural orbitals, form a complete orthonormal set. The associated eigenvalues  $n_{\alpha}$  called natural occupation numbers define the probability ( $0 \leq n_{\alpha} \leq 1$ ) of the natural orbital  $\psi_{\alpha}(\mathbf{r})$  occupation in the ground state  $\Psi$ . Within the NOR the Wigner transform of  $\rho(\mathbf{r}, \mathbf{r}')$  can be derived as follows:

$$f(\mathbf{k}_c, \mathbf{r}) = \sum_c n_c h_c^{NO}(\mathbf{k}_c, \mathbf{r}) = \sum_c n_c \int_0^{\infty} d\mathbf{s} e^{-i\mathbf{k}_c \mathbf{s}} \psi_c(\mathbf{r} + \mathbf{s}/2) \psi_c^*(\mathbf{r} - \mathbf{s}/2) \quad (7)$$

We would like to note that the summation in Eq. (7) is taken over all hole- as well as particle-state NO included in the calculation of the Wigner transform. In the present work we use the results for the natural orbitals and for the occupation numbers in  $^{40}\text{Ca}$  obtained in Ref. [18] within the JCM in its low-order approximation. As it has been already done in [5] for the s.p. wave functions, in the present work each NO  $\psi_c(\mathbf{r})$  is expanded in terms of the Gaussian-type basis function

$$\psi_c(\mathbf{r}) = \sum_{v=1}^N a_v^{(c)} \exp(-\kappa_v^2 r^2), \quad (8)$$

where  $N$  is the number of the basis functions,  $\kappa_v$  is given by a geometrical progression [19],  $\kappa_v = \kappa_1 (\kappa_N / \kappa_1)^{(v-1)/(N-1)}$ . The  $\{N, \kappa_1, \kappa_N\}$  are the input parameters. The expansion coefficients  $a_v^{(c)}$  are determined by linear fitting of the basis functions (8) to the numerical data for the natural orbitals. Then each partial Wigner transform is calculated in accordance with Eq. (2.39) in Ref. [5] and after applying Eq. (7) the total Wigner transform for the NOR of  $\rho(\mathbf{r}, \mathbf{r}')$  is obtained.

### 3.3 WT with LDA+SRC

It is well known that the inclusion of correlations in nuclear matter modifies the occupation probability predicted by the local density Fermi gas model. According to Ref. [20] one can introduce Wigner transform in a general way:

$$f(k_F(\mathbf{r}), k) = \Theta(k_F(\mathbf{r}) - k) + \delta f(k_F(\mathbf{r}), k), \quad (9)$$

where  $\Theta(k_F - k)$  corresponds to the WT of the LFG model, while  $\delta f(k_F, k)$  is entirely due to the effects of dynamical correlations induced by the NN interaction. The local Fermi momentum  $k_F(r)$  is related to the mass density through the relation

$$k_F(r) = \left[ \frac{3}{2} \pi^2 \rho(r) \right]^{1/3}. \quad (10)$$

By definition of  $k_F(r)$  one has  $\int \delta f(k_F(\mathbf{r}), k) d\mathbf{k} = 0$ . It was shown in [20] that for a finite nucleus the separation between mean-field contribution and correlation effects can be performed in an analogous way. For convenience more phenomenological procedure based on the results of

the lowest order cluster (LOC) approximation developed in [21] has been followed to evaluate explicitly the correlated term. Choosing a correlation function of the form

$$f(r) = 1 - e^{-\beta^2 r^2}, \quad (11)$$

the LOC gives for  $\delta f(k_F, k)$

$$\delta f(k_F(\mathbf{r}), k) = [Y(k, 8) - k_{dir}] \Theta(k_F(\mathbf{r}) - k) + 8 \left\{ k_{dir} Y(k, 2) - [Y(k, 4)]^2 \right\}, \quad (12)$$

where

$$c_\mu^{-1} Y(k, \mu) = \frac{e^{-\tilde{k}_+^2} - e^{-\tilde{k}_-^2}}{2\tilde{k}} + \int_0^{\tilde{k}_+} e^{-y^2} dy + sgn(\tilde{k}_-) \int_0^{|\tilde{k}_-|} e^{-y^2} dy \quad (13)$$

with

$$c_\mu = \frac{1}{8\sqrt{\pi}} \left( \frac{\mu}{2} \right)^{3/2}, \quad \tilde{k} = \frac{k}{\beta\sqrt{\mu}}, \quad \tilde{k}_\pm = \frac{k_F \pm k}{\beta\sqrt{\mu}}, \quad sgn(x) = \frac{x}{|x|}. \quad (14)$$

The quantity

$$k_{dir} = \frac{2k_F^3}{3\pi^2} \int (f(r) - 1)^2 d\mathbf{r} = \frac{1}{3\sqrt{2\pi}} \left( \frac{k_F}{\beta} \right)^3 \quad (15)$$

is the direct part of the Jastrow wound parameter.

### 3.4 WT with CDFM

The CDFM has been suggested in [22, 23, 24] as a model for studying characteristics of nuclear structure and nuclear reactions based on the local density distribution as a variable of the theory and using the essential results of the infinite nuclear matter theory. The model is introduced using the main ansatz of the generator coordinate method for the many-body function and the delta-function approximation for the overlap and energy kernels of the corresponding integral equation for the weight function. In the CDFM the Wigner distribution function can be written in the form:

$$f(\mathbf{r}, \mathbf{k}) = \int_0^\infty |f(x)|^2 \Theta(x - |\mathbf{r}|) \Theta(k_F(x) - |\mathbf{k}|) dx, \quad (16)$$

where the weight function  $f(x)$  in the generator coordinate method is determined under the condition

$$\int_0^\infty |f(x)|^2 dx = 1. \quad (17)$$

In the case of monotonically-decreasing density distributions ( $d\rho/dr \leq 0$ ) one can obtain a relation of the weight function  $f(x)$  with the density distribution:

$$|f(x)|^2 = -\frac{1}{\rho_0(x)} \left. \frac{d\rho(r)}{dr} \right|_{r=x}, \quad (18)$$

where

$$\rho_0(x) = 3A/4\pi x^3 \quad (19)$$

and the generator coordinate  $x$  is the radius of a sphere containing all  $A$  nucleons uniformly distributed in it (the so-called "flucton").

## 4 Results of calculations and discussion

The input data used in the calculations of Wigner transforms can be summarized as follows. The single-particle wave function in Eq. (5) were calculated using a Woods-Saxon potential with the radius parameter  $r_0=1.27$  fm and the surface diffuseness parameter  $a=0.67$  fm, including the isovector term and the Coulomb potential. The set  $\{N, \kappa_1, \kappa_N\}=\{20, 1, 0.1\}$  is taken for the WS potential and for the WT with NOR. For the correlation factor in Eq. (11) we adopt the same value  $\beta=1.1$  fm $^{-1}$  as in Ref. [20] which is taken from the microscopic nuclear matter calculations [25] but reproduces also well the results for the nucleon momentum distribution  $n(k)$  of finite nuclei. This value leads to  $k_{dir}=0.23$  [Eq. (15)]. In the CDFM method as well as in the LDA approach with SRC we use the nucleon density distribution  $\rho(r)$  of the Woods-Saxon shape with Negele's geometrical parameters [26]. The proton and the neutron densities are assumed to be given by  $(Z/A)\rho(r)$  and  $(N/A)\rho(r)$ , respectively. The local Fermi momentum  $k_F(r)$  was obtained from Eq. (10) using the same density distribution.

As for the other input data for the SCDW calculations, we use basically the same ones as in Ref. [8]. The global optical potentials based on Dirac phenomenology of Hama *et al.* [27] for protons and Ishibashi *et al.* [28] for neutrons were used. For a simplicity of the numerical calculations we neglect the spin-orbit coupling in the distorting potentials. The nonlocality correction for distorted waves and WS s.p. wave functions was taken into account using the Perey factor with range 0.85 [29]. An effective NN interaction in terms of  $G$  matrix parameterized by the Melbourne group [30] was employed. The two-nucleon scattering cross section in Eq. (2) is calculated using this  $G$  matrix. In addition to [8], an effective mass of a target nucleon  $m^*$  is used. We assume a simple WS form for the  $r$ -dependence of  $m^*$ . The latter at  $r=0$  was chosen to be  $m^* = 0.8m$  with a bare mass  $m$ .

Figure 1 shows the SCDW double differential cross sections with CDFM, LDA+SRC and WS for the  $^{12}\text{C}(p, p'x)$  reaction at 150 MeV incident and 80 MeV outgoing energies compared with two sets of experimental data [11, 12]. A good overall agreement with the data including backward angle region is obtained in the case of CDFM. The SCDW cross section calculated with WS drops down at backward angles, while those with LDA+SRC overestimates the experimental data. As will be discussed later, the main reason for this behavior is the different account for the high-momentum components of the nuclear Fermi motion. In Fig. 1 the contributions of individual multistep processes when CDFM is used for the same reaction are also plotted. One can see that proton emission via one-step process is dominant in the angular region from  $20^\circ$  to  $50^\circ$ . Contributions of two- and three-step processes become appreciable with increasing angles. The role of higher-step processes has been already seen in previous calculations [4, 5].

Comparisons between the cross sections calculated by using the Wigner transforms obtained with all theoretical methods considered and the measured cross sections for  $(p, p'x)$  on  $^{40}\text{Ca}$  at 186 MeV and 392 MeV incident energies are given in Fig. 2 and Fig. 3, respectively. Both figures confirm the fact that the cross sections at large angles depend strongly on the theoretical model used to describe the nuclear states. Fig. 2 shows a fair agreement of the CDFM and JCM results with the data for emission energy of 110 MeV and to less extent for energy of 130 MeV. At the same time, for emission energy of 150 MeV the WS result is able to reproduce the angular distribution at backward angles. Similar behavior can be seen from Fig. 3, where the double differential cross sections calculated with CDFM and that with JCM are in a good agreement with the experimental data. However, measurements over an extended range of backward angles can test the various methods and, hence, the role of NN correlations.

The improved description of the backward proton emission with the SCDW model by the use of realistic models for nuclear states can be explained by the difference in the momentum distribution of the target nucleons. Figure 4 shows the momentum distributions  $n(k)$  of  $^{12}\text{C}$  and  $^{40}\text{Ca}$  with CDFM, LDA+SRC, WS and JCM. One sees that  $n(k)$  calculated with all methods

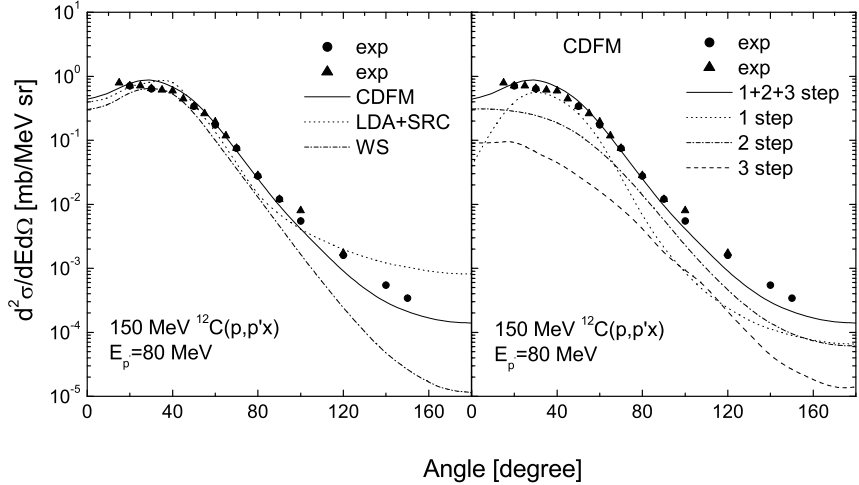


Figure 1: Comparison of SCDW calculations with measured double differential cross section for the reaction  $^{12}\text{C}(p, p'x)$  at 150 MeV incident and 80 MeV emission energies (solid circles from [11] and solid triangles from [12]). The calculations with CDFM (solid line), LDA+SRC (dotted line) and WS (dash-dotted) line are shown in the left panel. The CDFM calculations of the cross sections of one- (dotted line), two- (dash-dotted line) and three-step (dashed line) processes are shown in the right panel, where the solid line corresponds to their sum.

but not with the WS contain high-momentum components at momenta larger than  $1.5 \text{ fm}^{-1}$ . The LDA+SRC [20] and Jastrow method [18] account for short-range correlations, while the CDFM [22] takes into account mostly long-range correlations (LRC). The larger high-momentum component due to the stronger SRC when using LDA+SRC causes the larger cross sections at backward angles. Although  $n(k)$  calculated in this method fits well the experimental  $y$ -scaling data for  $^{12}\text{C}$  [31] at large momenta, the corresponding cross sections overestimate the data. Here we would like to note that the  $n(k)$  of  $^{40}\text{Ca}$  obtained after integration of the total WT  $f(\mathbf{k}, \mathbf{r})$  with JCM over  $\mathbf{r}$  is not given in Fig. 4 and it underestimates the one obtained in [18] at  $k \geq 2 \text{ fm}^{-1}$ . This is particularly due to the truncation of the particle-state NO's included in the calculation of the WT of  $^{40}\text{Ca}$ . On the other side, due to the lack of enough high-momentum components the angular distributions calculated with WS underestimate the data at backward angles. The nucleon momentum distributions obtained with CDFM for both nuclei presented in Fig. 4 also exhibit high-momentum components, though smaller than the ones corresponding to methods accounting for SRC. Fig. 4 clearly illustrates the strong dependence of backward proton production from  $(p, p'x)$  reactions on the momentum distribution of target nucleons.

In Fig. 5 the SCDW cross sections for  $^{90}\text{Zr}(p, p'x)$  at 160 MeV and emission energy of 120 MeV calculated with the CDFM, LDA+SRC and WS models are compared. Again a very good agreement with the experimental data over the forward, intermediate and backward angles is achieved when using the Wigner transform obtained from CDFM. In Fig. 6 the contributions of individual multistep processes for the same reaction and corresponding to the same models are plotted to show their variation with the scattering angle. It is seen that for this relatively large emission energy the one-step cross section calculated with LDA+SRC exceeds the experimental cross section for large angles. On the other hand, the one-step cross section obtained with WS drops at angles less than  $140^\circ$  underestimating the experimental cross section at backward angles.

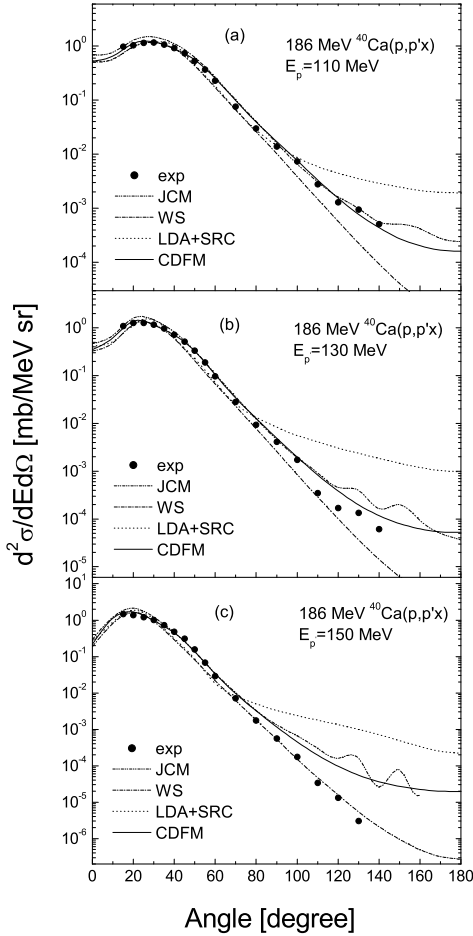


Figure 2: Comparison of SCDW calculations with measured double differential cross section for the reaction  $^{40}\text{Ca}(p, p'x)$  at 186 MeV incident and 110 MeV (a), 130 MeV (b) and 150 MeV (c) emission energies [13]. In each panel the calculations with CDFM (solid line), JCM (dash-double dotted line), LDA+SRC (dotted line) and WS (dash-dotted line) are shown.

From the analyses of high energy heavy ion collision and deep inelastic lepton-nucleus scattering, the following form of the nucleon momentum distribution has been proposed [10]:

$$n(k) = N[\exp(-k^2/p_0^2) + \varepsilon_0 \exp(-k^2/q_0^2) + \varepsilon_1 \exp(-k^2/q_1^2)], \quad (20)$$

where  $N$  is a normalization factor and the values of the parameters are determined to be  $p_0 = \sqrt{\frac{2}{5}}k_F$ ,  $\varepsilon_0 \cong 0.03$ ,  $q_0 \cong \sqrt{3}p_0$ ,  $\varepsilon_1 \cong 0.003$  and  $q_1 \cong 0.5 \text{ GeV}/c$ . The first term of Eq. (20) corresponds to single-particle contribution to  $n(k)$  in the mean-field approximation (MFA). It was noticed in [10] that the second term in Eq. (20) is due to the long-range correlations (L-type high momentum component) while the third term was supposed to be due to short-range correlations (S-type high momentum component). Moreover, as it was also noticed in Ref. [10] only the high-momentum component generated by the Hartree-Fock correlation should be included in the single scattering calculation. In order to reveal better the role of different NN correlations for the correct description of the backscattered proton spectra, we make in Fig. 7 a comparison between the nucleon momentum distributions calculated with CDFM and JCM and those calculated by using Eq. (20) in the case of  $^{12}\text{C}$  and  $^{40}\text{Ca}$  nuclei. Particularly, our

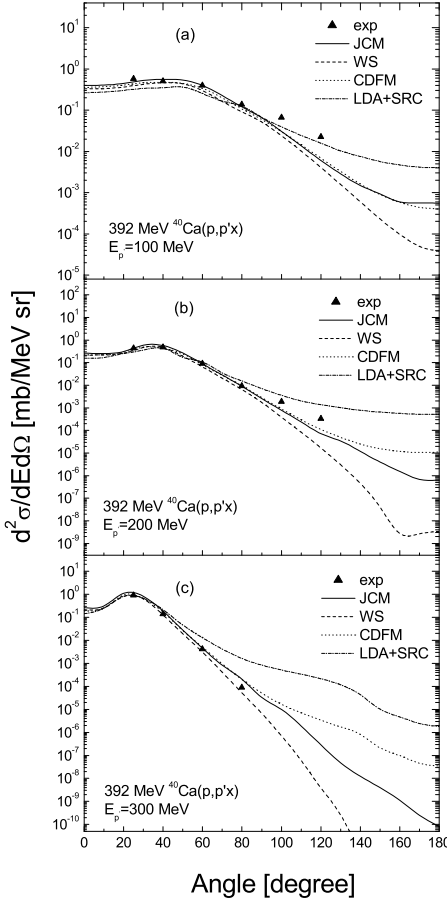


Figure 3: Comparison of SCDW calculations with measured double differential cross section for the reaction  $^{40}\text{Ca}(p, p'x)$  at 392 MeV incident and 100 MeV (a), 200 MeV (b) and 300 MeV (c) emission energies [14]. In each panel the calculations with CDFM (dotted line), JCM (solid line), LDA+SRC (dash-dotted line) and WS (dashed line) are shown.

interest is in the comparison of the high-momentum components which the different methods contain. It turns out from Fig. 7 that for  $k > 1.5 \text{ fm}^{-1}$  the curves corresponding to the inclusion only of the L-type term and CDFM have similar behavior (especially for  $^{12}\text{C}$ ), while the results when including only the S-type term and Jastrow method are close to each other. It is seen also from Fig. 7 that the contribution of the S-type term dominates in the total  $n(k)$  calculated by Eq. (20). Therefore, we suggest that the long-range correlations play an important role to the problem of backward proton production. This is confirmed by the good agreement obtained in [9] and by our results obtained with the use of Wigner transform with CDFM which lead to best description of the experimental cross sections over wide target mass number and emission energy regions.

## 5 Summary

The results of the present work can be summarized as follows:

- i) Double-differential cross sections of  $^{12}\text{C}(p, p'x)$ ,  $^{40}\text{Ca}(p, p'x)$  and  $^{90}\text{Zr}(p, p'x)$  reactions are

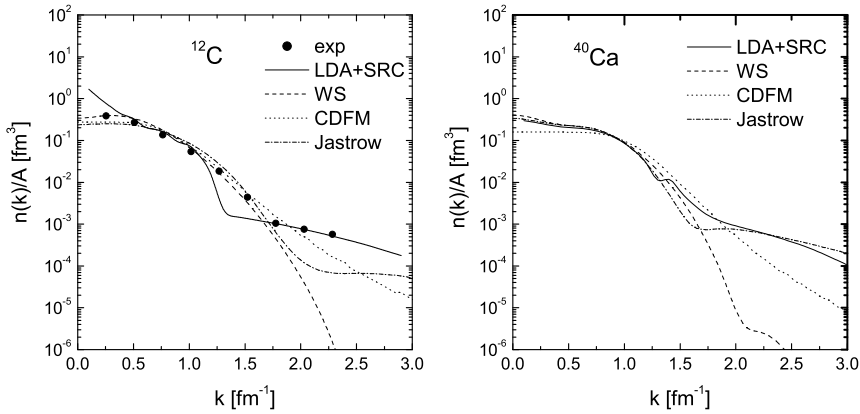


Figure 4: Comparison of nucleon momentum distributions  $n(k)$  (normalized to unity) of  $^{12}\text{C}$  and  $^{40}\text{Ca}$  calculated with CDFM (dotted line), LDA+SRC (solid line), WS (dashed line) and JCM [18] (dash-dotted line). The experimental data for  $n(k)$  of  $^{12}\text{C}$  are taken from [31].

calculated, using SCDW model and Wigner transform of the OBDM obtained with different approaches, in the incident energy range of 150–392 MeV. A good overall agreement with the experimental data is achieved including the backward angles region. These analyses show that the present SCDW model can describe successfully the MSD processes of  $(p, p'x)$  reactions over the wide range of target mass number and incident energies.

ii) It is found that the high-momentum components of the nucleon momentum distribution are most responsible for describing the angular distributions of the backscattered protons. Since CDFM leads to the best agreement with the experimental cross sections at wide emission energy region, it is demonstrated that the long-range correlations which are related to the collective nucleon motion are rather important than the short-range ones generated in the other correlation methods.

A more detailed study on the backward proton emission in the framework of the CDFM is in progress.

## 6 Acknowledgments

The authors wish to thank Professor A.A. Cowley for providing us the experimental data from Ref. [13]. One of the authors (MKG) is grateful to the JSPS's Postdoctoral Fellowships for foreign researchers. This work was partly supported by a Grant-in-Aid for Scientific Research of the Ministry of Education, Science and Culture (No. 14002042).

## References

- [1] Y.L. Luo and M. Kawai, Phys. Lett. **B235**, 211 (1990); Phys. Rev. C **43**, 2367 (1991).
- [2] M. Kawai and H.A. Weidenmüller, Phys. Rev. C **45**, 1856 (1992).
- [3] Y. Watanabe and M. Kawai, Nucl. Phys. **A560**, 43 (1993).

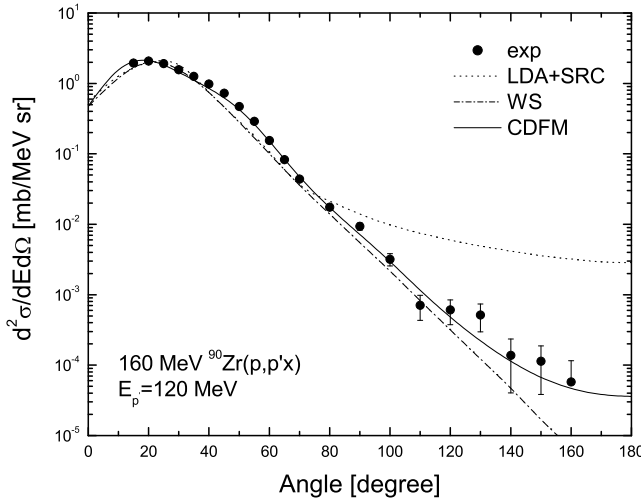


Figure 5: Comparison of SCDW calculations with measured double differential cross section for the reaction  $^{90}\text{Zr}(p, p'x)$  at 160 MeV incident and 120 MeV emission energies [15]. The calculations with CDFM (solid line), LDA+SRC (dotted line) and WS (dash-dotted line) are shown.

- [4] Y. Watanabe, R. Kuwata, S. Weili, M. Higashi, H. Shinohara, M. Kohno, K. Ogata, and M. Kawai, Phys. Rev. C **59**, 2136 (1999).
- [5] S. Weili, Y. Watanabe, M. Kohno, K. Ogata, and M. Kawai, Phys. Rev. C **60**, 064605 (1999).
- [6] K. Ogata, M. Kawai, Y. Watanabe, Sun Weili, and M. Kohno, in *Proceedings of the International Symposium on Nuclear Many-Body and Medium Effects in Nuclear Interactions and Reactions*, Fukuoka, 2002, edited by K. Hatanaka *et al.*, (World Scientific, Singapore, 2003), p. 231.
- [7] K. Ogata, M. Kawai, Y. Watanabe, Sun Weili, and M. Kohno, Phys. Rev. C **60**, 054605 (1999).
- [8] K. Ogata, Y. Watanabe, Sun Weili, M. Kohno, and M. Kawai, Nucl. Phys. **A703**, 152 (2002).
- [9] Y. Haneishi and T. Fujita, Phys. Rev. C **33**, 260 (1986); Phys. Rev. C **35**, 70 (1987).
- [10] T. Fujita, Nucl. Phys. **A457**, 657 (1986).
- [11] G.F. Steyn, A.A. Cowley, Y. Watanabe, Sun Weili, S.V. Förtzsch, and J.J. Lawrie, in *Proceedings of the International Conference on Nuclear Data for Science and Technology*, Tsukuba, 2001, edited by K. Shibata, v.1, p. 291.
- [12] S.V. Förtzsch, A.A. Cowley, J.V. Pilcher, D.M. Whittal, and J.J. Lawrie, Nucl. Phys. **A485**, 258 (1988).
- [13] S.W. Steyn, PhD thesis, University of Stellenbosch (1997).

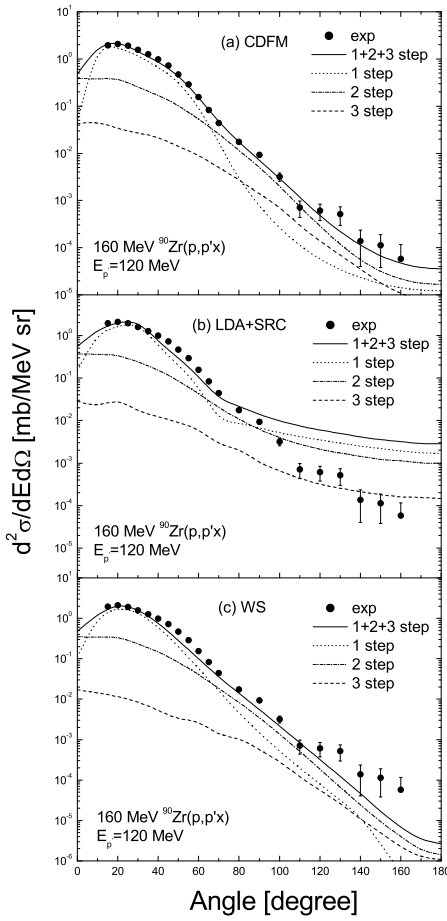


Figure 6: Comparison of SCDW calculations with measured double differential cross section for the reaction  $^{90}\text{Zr}(p, p'x)$  at 160 MeV incident and 120 MeV emission energies [15]. The calculations with CDFM, LDA+SRC and WS are shown in panels (a), (b) and (c), respectively. In each panel the cross sections of one- (dotted line), two- (dash-dotted line) and three-step (dashed line) processes are shown. The solid line corresponds to their sum.

- [14] A.A. Cowley, G.F. Steyn, Y. Watanabe, T. Noro, K. Tamura, M. Kawabata, K. Hatanaka, H. Sakaguchi, H. Takeda, and M. Itoh, Phys. Rev. C **62**, 064604 (2000).
- [15] W.A. Richter, A.A. Cowley, G.C. Hillhouse, J.A. Stander, J.W. Koen, S.W. Steyn, R. Lindsay, R.E. Julies, J.J. Lawrie, J.V. Pilcher, and P.E. Hodgson, Phys. Rev. C **49**, 1001 (1994).
- [16] C. Mahaux and R. Sartor, Nucl. Phys. **A481**, 381 (1988) (and references therein).
- [17] R. Jastrow, Phys. Rev. **98**, 1479 (1955).
- [18] M.V. Stoitsov, A.N. Antonov, and S.S. Dimitrova, Phys. Rev. C **48**, 74 (1993).
- [19] M. Kamimura, Phys. Rev. A **38**, 621 (1988).
- [20] S. Stringari, M. Traini, and O. Bohigas, Nucl. Phys. **A516**, 33 (1990).

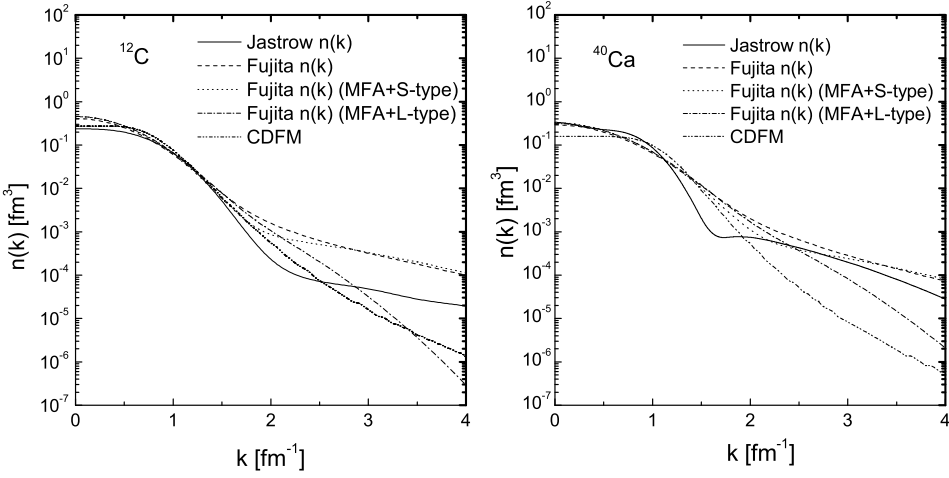


Figure 7: Comparison of nucleon momentum distributions  $n(k)$  (normalized to unity) of  $^{12}\text{C}$  and  $^{40}\text{Ca}$  calculated with CDFM (dash-double dotted line), JCM [18] (solid line) and by using Eq. (20): total  $n(k)$  (dashed line), MFA+S-type terms (dotted line) and MFA+L-type terms (dash-dotted line).

- [21] M.F. Flynn, J.W. Clark, R.M. Panoff, O. Bohigas, and S. Stringari, Nucl. Phys. **A427**, 253 (1984).
- [22] A.N. Antonov, V.A. Nikolaev, and I.Zh. Petkov, Bulg. J. Phys. **6**, 151 (1979); Preprint ICTP IC/78/152, Trieste (1978); Z. Phys. **A297**, 257 (1980).
- [23] A.N. Antonov, P.E. Hodgson, and I.Zh. Petkov, *Nucleon Momentum and Density Distributions in Nuclei* (Clarendon Press, Oxford, 1988).
- [24] A.N. Antonov, P.E. Hodgson, and I.Zh. Petkov, *Nucleon Correlations in Nuclei* (Springer-Verlag, Berlin, 1993).
- [25] S. Fantoni and V.R. Pandharipande, Nucl. Phys. **A427**, 473 (1984).
- [26] J.W. Negele, Phys. Rev. C **1**, 1260 (1970).
- [27] S. Hama, B.C. Clark, E.D. Cooper, H.S. Sherif, and R.L. Mercer, Phys. Rev. C **41**, 2737 (1990); E.D. Cooper, S. Hama, B.C. Clark, and R. L. Mercer, *ibid.*, **47**, 297 (1993).
- [28] K. Ishibashi, S. Maruyama, and N. Shigyo, in *Proceedings of a Specialists Meeting on Nucleon-Nucleus Optical model up to 200 MeV*, Bruyeres-le-Chatel, France, 1996, p. 91 (1997).
- [29] F.G. Perey and B. Buck, Nucl. Phys. **32**, 353 (1962).
- [30] K. Amos, P.J. Dortmans, H.V. von Geramb, S. Karatagliidis, and J. Raynal, Adv. Nucl. Phys. **25**, 275 (2000).
- [31] C. Ciofi degli Atti, E. Pace, and G. Salmè, Phys. Rev. C **43**, 1155 (1991).